Neurobiology of Disease 124 (2019) 57–66

Contents lists available at ScienceDirect

Neurobiology of Disease

journal homepage: www.elsevier.com/locate/ynbdi

Mitochondrial dysfunction in preclinical genetic prion disease: A target for preventive treatment?

Guy Keller[a,c,1], Orli Binyamin[a,c,1], Kati Frid[a,c], Ann Saada[b,c], Ruth Gabizon[a,c,*]

[a] Department of Neurology, The Agnes Ginges Center for Human Neurogenetics, Israel
[b] Department of Genetics and Metabolic Diseases, The Monique and Jacques Roboh Department of Genetic Research, Hadassah-Hebrew University Medical Center, Israel
[c] Medical School, The Hebrew University, Jerusalem, Israel

ABSTRACT

Mitochondrial malfunction is a common feature in advanced stages of neurodegenerative conditions, as is the case for the accumulation of aberrantly folded proteins, such as PrP in prion diseases. In this work, we investigated mitochondrial activity and expression of related factors vis a vis PrP accumulation at the subclinical stages of TgMHu2ME199K mice, modeling for genetic prion diseases. While these mice remain healthy until 5–6 months of age, they succumb to fatal disease at 12–14 months. We found that mitochondrial respiratory chain enzymatic activates and ATP/ROS production, were abnormally elevated in asymptomatic mice, concomitant with initial accumulation of disease related PrP. In parallel, the expression of Cytochrome c oxidase (COX) subunit IV isoform 1(Cox IV-1) was reduced and replaced by the activity of Cox IV isoform 2, which operates in oxidative neuronal conditions. At all stages of disease, Cox IV-1 was absent from cells accumulating disease related PrP, suggesting that PrP aggregates may directly compromise normal mitochondrial function. Administration of Nano-PSO, a brain targeted antioxidant, to TgMHu2ME199K mice, reversed functional and biochemical mitochondrial functions to normal conditions regardless of the presence of misfolded PrP. Our results therefore indicate that in genetic prion disease, oxidative damage initiates long before clinical manifestations. These manifest only when aggregated PrP levels are too high for the compensatory mechanisms to sustain mitochondrial activity.

1. Introduction

The hallmark of late onset neurodegenerative diseases, such as Alzheimer's (AD), Parkinson (PD) and Creutzfeldt Jacob (CJD) diseases, is the accumulation over time and disease advance of aberrantly folded key disease proteins (Kovacs and Budka, 2008), either after pathological refolding of the wild-type form, or by the spontaneous misfolding or a mutant protein, as is the case for carriers of pathogenic mutations linked to genetic neurodegenerative diseases (Brown and Mastrianni, 2010; Scheckel and Aguzzi, 2018). Altered conformation is accompanied by oxidation of the aberrant key proteins and lipids around it, as well as impairment of the proteasomal and lysosomal pathways (Redmann et al., 2016). Impaired mitochondrial activity, which may result from oxidative stress and inhibition of mitochondrial turnover, has been reported mostly at late stages of disease both in humans and in animal models for both prion and AD (Di Carlo et al., 2012; Faris et al., 2017). Declined mitochondrial functionality is also associated with aging, probably due to reduction of both autophagic activity and mitochondrial biogenesis (Cuervo, 2008; Herbener, 1976). In neurodegenerative diseases, several investigations demonstrated oxidative damage to key enzymes involved in energy metabolism, mitochondrial proteins and proteasomal components (Twig and Shirihai, 2011). Whether the accumulation of misfolded key disease proteins directly cause mitochondrial dysfunction and oxidative stress is unknown at this stage.

To elucidate the mechanism of disease initiation in late onset genetic diseases, we set to investigate the cross talk between the early steps of pathogenic mutant proteins accumulation, oxidative stress and mitochondrial dysfunction in brains of subclinical subjects. While this cannot be done in humans, transgenic mice models of neurodegenerative genetic diseases offer the opportunity to investigate these questions (Ashe, 2001; Fainstein et al., 2016; Recasens et al., 2017). To this effect, we studied mitochondrial respiratory chain (MRC) enzymatic activity, ATP and reactive oxygen species (ROS) production as well as expression of relevant enzymes and oxidation factors in different ages and disease status of TgMHu2ME199K mice, modeling for genetic CJD linked to the E200K PrP mutation (Friedman-Levi et al., 2011), and compared those to levels of disease related PrP accumulation and disease scores. Indeed, while the TgMHu2ME199K mice remained asymptomatic until 5–6 months of age, their brains presented considerable levels of disease related PrP forms already at 1.5 months of age (Frid et al., 2018). Subsequently, and while neurological and cognitive dysfunction was apparent only from 6 to 7 months of age onward, the levels of disease related PrP at this time point were already at their maximum (Binyamin

* Corresponding author at: Department of Neurology, The Agnes Ginges Center for Human Neurogenetics, Israel.
E-mail address: gabizonr@hadassah.org.il (R. Gabizon).
[1] Equal contribution.

https://doi.org/10.1016/j.nbd.2018.11.003
Received 13 September 2018; Accepted 9 November 2018
Available online 10 November 2018
0969-9961/

et al., 2017a). TgMHu2ME199K mice deteriorate to a terminal stage only at 12–15 months, concomitant with significant neuronal death. This suggests that while expression of mutant PrP forms prone to aggregation, as is the case for E200K PrP (Wang et al., 2016) may trigger the initiation of the neuropathological process, other events may determine the time point of disease onset and the subsequent rate of aggravation. To further understand the kinetics of neurodegeneration, we looked into mitochondrial markers in young and adult TgMHu2ME199K mice after administration of Nano-PSO, which anti-prion mechanism relates to oxidative stress and is independent from PrP accumulation (Binyamin et al., 2017a; Mizrahi et al., 2014).

We show here that while TgMHu2ME199K mice did not present any disease signs until 5–6 months of age, oxidative phosphorylation (OXPHOS) markers, such as ROS and ATP as well as electron transport chain enzymes activities were significantly elevated at 1.5 months of age, suggesting a stress situation. We also demonstrate that from very early age there was a significant reduction in the expression of the COX4–1 isoform and concomitant elevation of COX IV-2, a COX-IV isoform expressed at toxic and degenerative conditions levels (Arnold, 2012), indicating a compensatory mechanism is already in place. Our results also show that Cox IV-1 was not co-expressed with disease related PrP, suggesting that the presence of PrP aggregates may compromise normal mitochondrial function in cells. Contrarily to the asymptomatic stage, the activity of most mitochondrial parameters were reduced in older and sick TgMHu2ME199K mice, concomitantly with neuronal death, indicating the correction system operating at early age could no longer compensate and inhibit clinical disease. Interestingly, treatment with Nano-PSO at both ages restored mitochondrial activity to wt levels, and in addition allowed for the co-expression of Cox 4–1 and disease related PrP, suggesting “cleaning” ROS from the cells may help delay disease manifestations.

2. Materials and methods

2.1. Nano-PSO

Preparation of Nano-PSO self-emulsifying formulation was as previously described (Binyamin et al., 2017b) and is defined in patent no. 14/523,408.

2.2. Animal studies

This study was carried out in strict accordance with the recommendations in the Guide for the Care and Use of Laboratory Animals of the National Institutes of Health. All animal experiments were conducted under the guidelines and supervision of the Hebrew University Ethical Committee, which approved the methods employed in this project (Permit Number: MD-15-14,462-5).

2.3. Administration of Nano-PSO to TgMHu2ME199K mice

Nano-PSO was administrated to groups of 6–8 young and adult mice for 2 weeks by adding a self-emulsion formulations into drinking water to final concentration of 1.6% oil/ml as previously described (Binyamin et al., 2017b). In some cases, brain slices from TgMHu2ME199K mice treated continuously from birth to 9 months of age were also tested in immunohistochemistry experiments.

2.4. Pathological examinations and immunocytochemistry

Histological evaluations were performed on paraffin-embedded sections of brain samples form wt or TgMHu2ME199K mice at different ages. Sections were stained by immunofluorescence with an array of designated antibodies. αCOX IV (ab202554) rabbit monoclonal antibody (abcam), raised against a human COX IV1 peptide which in mice recognizes only COX IV1; αCOX IV (ab33985) mAB raised against a different human COX IV1 peptide which also recognizes mouse COX IV1 (activity inhibited only with designated COXIV1 peptide); α CoxIV 2 rabbit polyclonal antibody (Proteintech) raised against total human COX IV 2, which may recognize both COX IV isoforms in mice (70% homology with mouse Cox IV 2, 46 homology with mouse COX IV 1); α TOM20 antibody (GeneTex), α Proteasome 20S C2 antibody (abcam); α Nrf2 antibody (ab89443) and α-PrP pAb RTC (Canello et al., 2010; Mizrahi et al., 2014). As most α-PrP antibodies, pAb RTC recognizes disease related PrP forms either after PK digestion or after denaturation (Kovacs et al., 2011; Serban et al., 1990). Secondary antibodies coupled to Alexa Fluor 488 and 568 were used (abcam). Nuclei were labeled with DAPI Fluoromount (Vector Laboratories) Confocal analysis was performed with Nikon A1R Confocal Laser Microscope System using the NIS-Elements C control software.

2.5. Western blot analysis

Brain extracts from TgMHu2ME199K mice at the designated time points were homogenized at 10% (*W/V*) in 10 mM Tris–HCl, pH 7.4 and 0.3 M sucrose. For Proteinase K digestions, 200 μg of 10% brain homogenates were extracted with 2% sarcosyl on ice before incubation with 40 mg/ml Proteinase K for 30 min at 37 °C. Samples were subsequently boiled in the presence of SDS, subjected to SDS PAGE and immunoblotted with α-PrP pAb RTC (Canello et al., 2010).

2.6. Mitochondrial isolation

Mitochondria were isolated from brain by glass-teflon homogenization in isolation buffer (sucrose 250 mM, EDTA acid 2 mM, Tris 10 mM, heparin 50 lg/ml pH 7.4). followed by centrifugation at 4 °C, for 10 min at 1000 ×*g* to remove the nuclei and the supernatant was centrifuged for 10 min at 14,000 ×*g* the mitochondrial enriched pellet was washed once and suspended in isolation buffer (Saada et al., 2003).

The enzymatic activities of respiratory chain complexes were measured in isolated mitochondria at 37 °C by standard spectrophotometric methods (All chemicals were purchased from Sigma-Aldrich,Israel). Complex I was measured as rotenone (3 μM) sensitive NADH-CoQ reductase monitoring the oxidation of 0.1 mM NADH at 340 nm of coenzyme 50uM Q1 in 10 mM Tris-HCl buffer at pH 7.8 the presence of 0.2 M KCN (Saada et al., 2004). Complex II was measured as succinate dehydrogenase (SDH) based on the 20 mM succinate mediated 1.6 mM phenazine methosulfate reduction of 50 μM dichloroindophenol at 600 nm in 50 mM potassium phosphate buffer pH 7.4 in the presence of 0.2 M KCN (Reisch and Elpeleg, 2007). Complex II + III was measured as succinate cytochrome *c* reductase in the presence 20 mM succinate and following the reduction of 50 μM oxidized cytochrome *c* at 550 nm in the presence of the presence of 0.2 M KCN and 3 μM Rotenone. Complex IV (COX, cytochrome *c* oxidase) was measured by following the oxidation of 25 μM reduced cytochrome *c* at 550 nm (Rustin et al., 1994). Citrate synthase (CS), a ubiquitous mitochondrial matrix enzyme, serving as a control, was measured in the presence of 0.3 mM acetylCoA and 0.5 mM oxaloacetate by monitoring the liberation of CoASH coupled to 1 mM 5′,5′-dithiobis (2-nitrobenzoic) acid at 412 nm in 100 mM Tris-HCl pH 8.1 (Reisch and Elpeleg, 2007).

2.7. Mitochondrial ATP production

ATP production in freshly isolated mitochondria was measured by luciferin-luciferase in assay buffer (5 mM K2HPO4, 10 mM, 100 mM KCl, 5 MgCl2, 0.005 EDTA, 75 mM mannitol, 25 mM sucrose and 0.6 mg/mg fatty acid free bovine serum albumin, at pH 7.4. containing 1 mM glutamate and 1 mM malate. The reaction was started by the addition of 0.25 mM ADP. After 5 min incubation at 25 °C the reaction was terminated and ATP content was measured according to the manufacturer's instructions (ATPlite® luminescence assay system, Perkin Elmer Waltham MA, USA). Luminescence measurements were

performed with a Synergy HT microplate reader (Bio-Tek instruments, Vinoosky VT, USA). The amount of ATP formed was calculated on the basis of a standard curve constructed on each separate occasion.

(Shufaro et al., 2012)

2.8. Mitochondrial ROS production

Mitochondrial ROS production was determined spectrofluorometricaily using H2DCF-DA. Mitochondria (0.25 mg of protein/ml) were incubated at 30 °C with 2 μM H_2DCF-DA and 10 mM succinate. DCF fluorescence was monitored using a Synergy HT microplate reader (Bio-Tek Instruments, Vinoosky VT, USA) at an excitation wavelength of 485 nm and emission wavelength of 520 nm (Degli Esposti, 2002).

2.9. Real-time PCR

RNA samples (3–6 subjects of each group) were isolated using standard procedures. cDNA was produced from 13.3 ng/μl total RNA with a qScript cDNA Synthesis Kit (Quanta Biosciences, Gaithersburg, MD, USA), according to the manufacturer's instructions. Real-time PCR amplification and relative quantification were analyzed with StepOne real time RT PCR (Life Technologies). The reaction mix included 1 μl cDNA, and 300 nmol/l of each of the following primers (Biosearch Technologies Inc.): *UBC*. 5′ – CAG CCG TAT ATC TTC CCA GAC – 3′ (forward) 5′ – CTC AGA GGG ATG CCA GTA ATC TA – 3′ (reverse) Nrf1. 5′ – CCA CAG GAG GTT AAT TCA GAG CT – 3′ (forward) 5′ – ATG CCC GAA GCT GAG CCT – 3′ (reverse) and 5 μl of SYBR green mix (Perfecta Syber Green Fast Mix ROX, Quanta Biosciences) in a total 10 μl volume. The fold changes of the target mRNAs were normalized to UBC. Then the fold changes of each mRNA were calculated based on the ratio between the analyzed TgMHu2ME199K/wild type tissues, as indicated. The experiment was in triplicate and the results are presented as the mean ± SD.

2.10. Statistical studies

Analyses of mitochondrial activity were performed with the Microsoft Excel software (2010). The differences between experimental groups were assessed by one-way analysis of variance followed by the paired two-tailed Student's *t*-test.

Quantification of pathology immunostaining was performed by measuring the stain-positive area in different fields at a magnification ×20. Stained pixels were measured and calculated using image pro analyzer 3D software, Media Cybernetics.

3. Results

3.1. Increased mitochondrial activity in young asymptomatic TgMHu2ME199Kmice

Enriched mitochondrial fractions from brains of each wt, TgMHu2ME199K and 2 weeks Nano-PSO treated TgMHu2ME199K mouse initiated either at 1 or 10 months of age were tested for ROS and ATP production, as well as for the activities of selected MRC enzymes. Enzymatic activities as well as levels of ROS and ATP were normalized for cytochrome synthase (CS) activity, to account for possible differences in mitochondrial preparation. The levels of statistical significance of differences between results between the groups was determined by the paired two-tailed Student's *t*-test.

The results described in Fig. 1 show that MRC enzymatic activities (Complex I, Complex II + III and Complex IV) in the brain mitochondrial fractions of young and asymptomatic TgMHu2ME199K mice were elevated as compared to those of wt mice as well as those of TgMHu2ME199K mice treated for 2 weeks with Nano-PSO (Fig. 1a-c). ROS and ATP production levels (Fig. 1c-d) were also elevated in the untreated young Tg brains. These results suggest the young and asymptomatic Tg mice already suffer from pathological energy shortage which may be corrected by elevated levels of mitochondrial activity accompanied by elevated ROS production. Fig. 1 also shows that, except for the activity of Complex IV (panel c), mitochondrial OXPHOS parameters were reduced in older and sick TgMHu2ME199K mice, as compared to wt and to Nano-PSO treated Tgs. Interestingly, sick TgMHu2ME199K samples present decreased ROS production indicating that the elevated ROS production in young mice may result from increased mitochondrial activity rather than from brain dysfunction. Indeed, previous studies have shown that at 10 months old TgMHu2ME199K mice, neuronal death was well established, suggesting remaining neurons may suffer and be approaching an apoptotic state (Fainstein et al., 2016; Mizrahi et al., 2014). A short treatment with Nano-PSO (2 weeks) restored mitochondrial enzymatic activity to normal levels at both asymptomatic and pre-asymptomatic mice. This is consistent with our concept that Nano-PSO administration may normalize/modulate ROS levels in the brain (Binyamin et al., 2017a; Binyamin et al., 2015).

3.2. Nano-PSO treatment prevents age-related reduction of TOM 20 levels in mitochondrial membranes of TgMHu2ME199K mice

Next, we immunostained brain sections of wt, Tgs and Nano-PSO treated young and old TgMHu2ME199K mice with an α TOM 20 antibody. TOM, the translocase of the outer membrane (Walther and Rapaport, 2009), is part of a multi-subunit complex that translocate mitochondrial proteins from the cytosol into the mitochondria, and its levels represent mitochondrial content in cells (Thornton et al., 2010). TOM20 was also shown to be reduced in aging, and aging related diseases, such as macular degeneration (Cano et al., 2014). Fig. 2 shows that in young mice, TOM20 levels were mostly the same for wt and TgMHu2ME199K mice. However, TOM20 levels were significantly reduced in adult TgMHu2ME199K mice, representing an accelerated aging process of mitochondria. This can be observed both in the pictures themselves and even more so in the quantitation of their fluorescence signal (see legend of Fig. 2). Interestingly, Tom20 levels in the cortex of TgMHu2ME199K mice treated with Nano-PSO for 2 weeks were higher than those of wt mice, while in the hippocampus this effect was observed only in TgMHu2ME199K mice treated continuously with Nano-PSO since their day of birth. This is probably so since in older mice treated for 2 weeks, Nano-PSO can only reduce ROS levels and allow for mitochondrial biogenesis at cells which are still alive, while in the long-term treatment, Nano-PSO significantly postponed neuronal death (Binyamin et al., 2017a).

3.3. COX IV-1 expression is significantly reduced in TgMHu2ME199K mice

The only enzyme of the respiratory chain which activity was preserved in adult/sick TgMHu2ME199K brains was Complex IV (cytochrome oxidase). This enzyme, which comprises 13 subunits, catalyzes the final step in the mitochondrial electron transfer chain and is regarded as one of the major regulation sites for oxidative phosphorylation (Arnold, 2012). This regulatory mechanism mainly stems from the relative activity of both COX IV isoforms. The activity of the COX IV-I subunit is inhibited by high ATP levels, therefore enabling regulation of ATP synthesis to the cell energy demands. However, under oxidative stress and degenerative conditions, COX IV-1 is replaced by COX IV-2 in the cytochrome oxidase complex (Horvat et al., 2006). This isoform switch is subject to ATP feedback inhibition of COX, resulting in the increase of total COX activity and ATP production in neural cells, independently from the required cellular energy level. Concomitantly, ROS production is increased. This ensures the ATP demands of neural cells under pathological conditions, but at the expense of elevated oxidative stress (Arnold et al., 1997). To investigate if this known phenomena occurs in the TgMHu2ME199K mice, we studied the expression of the COX IV isoforms in the brains of wt and

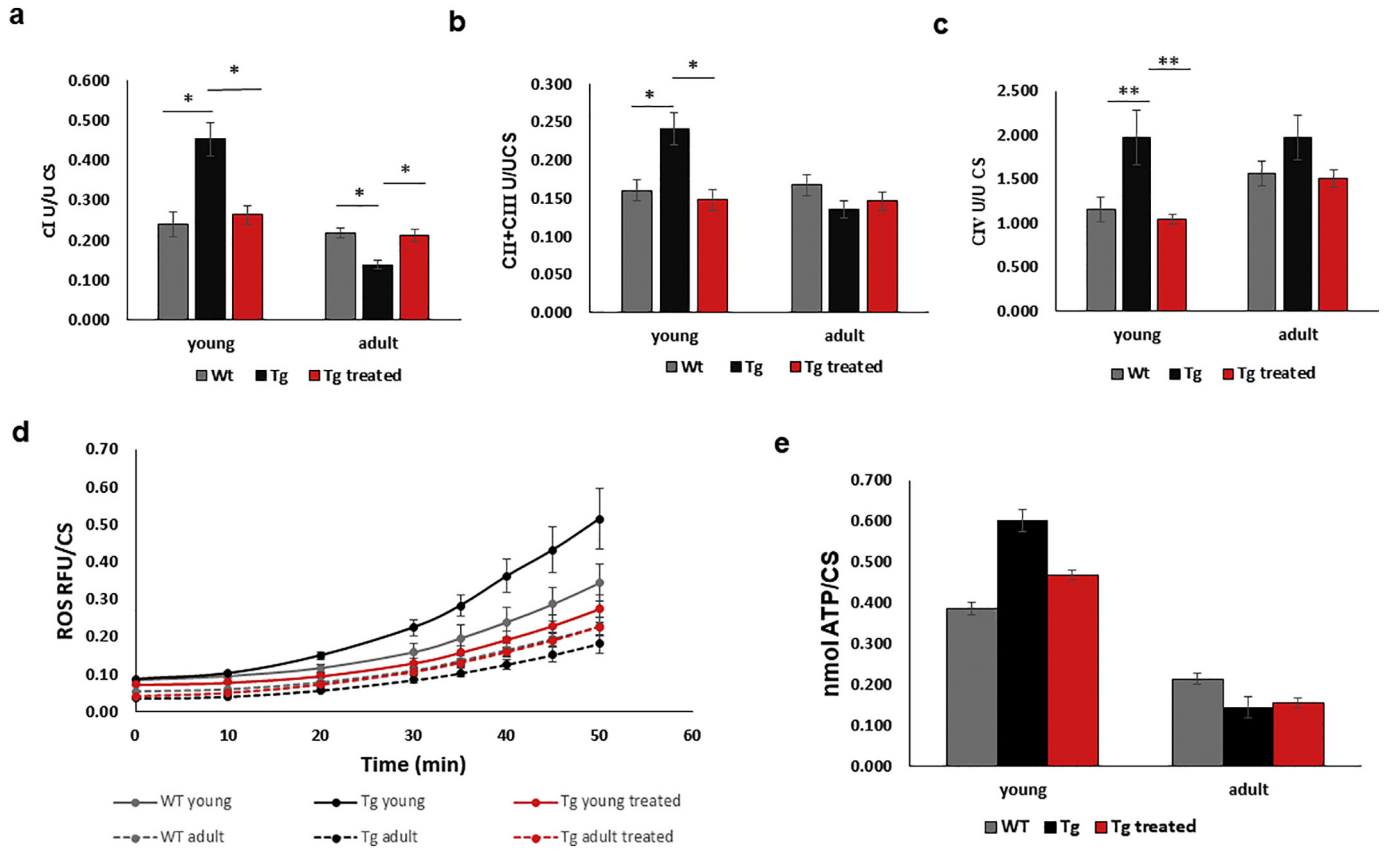

Fig. 1. Impaired mitochondrial activity in TgMHu2ME199K mice.
Activity of mitochondrial enzymes was measured as described in the methods in enriched brain mitochondrial fractions of young and adult WT, TgMHu2ME199K and 2 weeks Nano-PSO treated TgMHu2ME199K mice. (a) complex I activity (b) complex CII + CIII activity (c) complex IV activity (d) ROS production (e) ATP levels. (a-c) data are means ± SEM (n = 6/groups) *P < .01; **P < .001 (d) data are means ± SEM (WT young n = 6, Tg young n = 4, Tg young treated n = 6, WT adult n = 3, Tg adult n = 4 and Tg adult treated n = 6) (e) data are means ± SEM (n = 2/groups).

TgMHu2ME199K mice at different ages by immunostaining brain sections with several α-COX IV antibodies, recognizing either COXIV-1 or COXIV 1 and 2 (see Methods section). Fig. 3a shows that the COX-IV1 staining was slightly reduced in newborn TgMHu2ME199K mice (5 days), as compared to wt mice of the same age, it was significantly reduced in young (1.5 m) Tgs, eventhough these mice, as is the case for the newborns, were totally asymptomatic. In the older and severely affected TgMHu2ME199K mice (10.5 m), immunostaining of COX IV-1 was almost abolished (see also quantitation in the figure legends). Interestingly, both young and adult TgMHu2ME199K mice treated with Nano-PSO for 2 weeks presented elevated levels of COX IV-1, significantly higher than those of wt mice. Next, parallel slides were immunostained with a polyclonal antibody raised against full length human COX-IV 2, which, based on sequence comparison by blast (NCBI), may react also with the mouse COX-IV 1 isoform. Panel b shows that, in contrast to the result obtained with the Cox IV1 antibodies, the levels of COX IV recognized by this antibody were mostly similar in samples of the same age, indicating that COX IV2 activity may compensate for the absence of COX IV-1. This compensatory mechanism could also explain why COX activity (Fig. 1) was elevated in the brains of adult mice suffering from the disease.

3.4. COX IV-1 is not co-expressed with disease related PrP

In order to better understand the events leading to the COX-IV switch in brains from TgMHu2ME199K mice, we co-stained brain sections of Nano-PSO treated and untreated TgMHu2ME199K brains at the asymptomatic and disease state for both COX IV-1 and disease related PrP [pAb anti PrP RTC (Canello et al., 2010)]. Fig. 4a shows that in the untreated TgMHu2ME199K brains of both young and adult mice, COX IV -1 (red) is absent from cells accumulating disease related PrP (green). This can be seen more in detail in panel b (larger magnification). This was not the case for TgMHu2ME199K mice treated for 2 weeks with Nano-PSO, where the co-expression of both proteins in the same cells was clearly visible. Hence, our results suggest that brain targeted antioxidant reagents such as Nano-PSO may restore normal COX-IV 1 expression. We may therefore assume that early expression and accumulation of disease related PrP in TgMHu2ME199K mice may induce the COX IV isoform switch in the mitochondria. Subsequently, the age dependent increase in PrP accumulation may further contributes to mitochondrial malfunction eventually leading to cell death. The time lag between initial mitochondrial stress and cell death may be long and depend on the kinetics of PrP accumulation in the specific subject and the levels of mitochondrial activity compensation. As further evidence for this possible mechanism, we show that reduction of ROS levels by brain targeted antioxidants such as Nano-PSO can restore COX-IV 1 expression, concomitant with delay of disease aggravation and neuronal death, even in the presence of high levels of disease related PrP (Binyamin et al., 2017a).

3.5. Disease related PrP may induce reduction of NRF1 and NRF2 expression levels

To investigate further the correlation between mitochondrial function under stress and the accumulation of disease related PrP forms, we looked in the brains of TgMHu2ME199K mice of different ages for the expression levels of NRF-1, a potent enhancer of mitochondrial biogenesis (Wang et al., 2014; Li et al., 2017), and a coordinator of

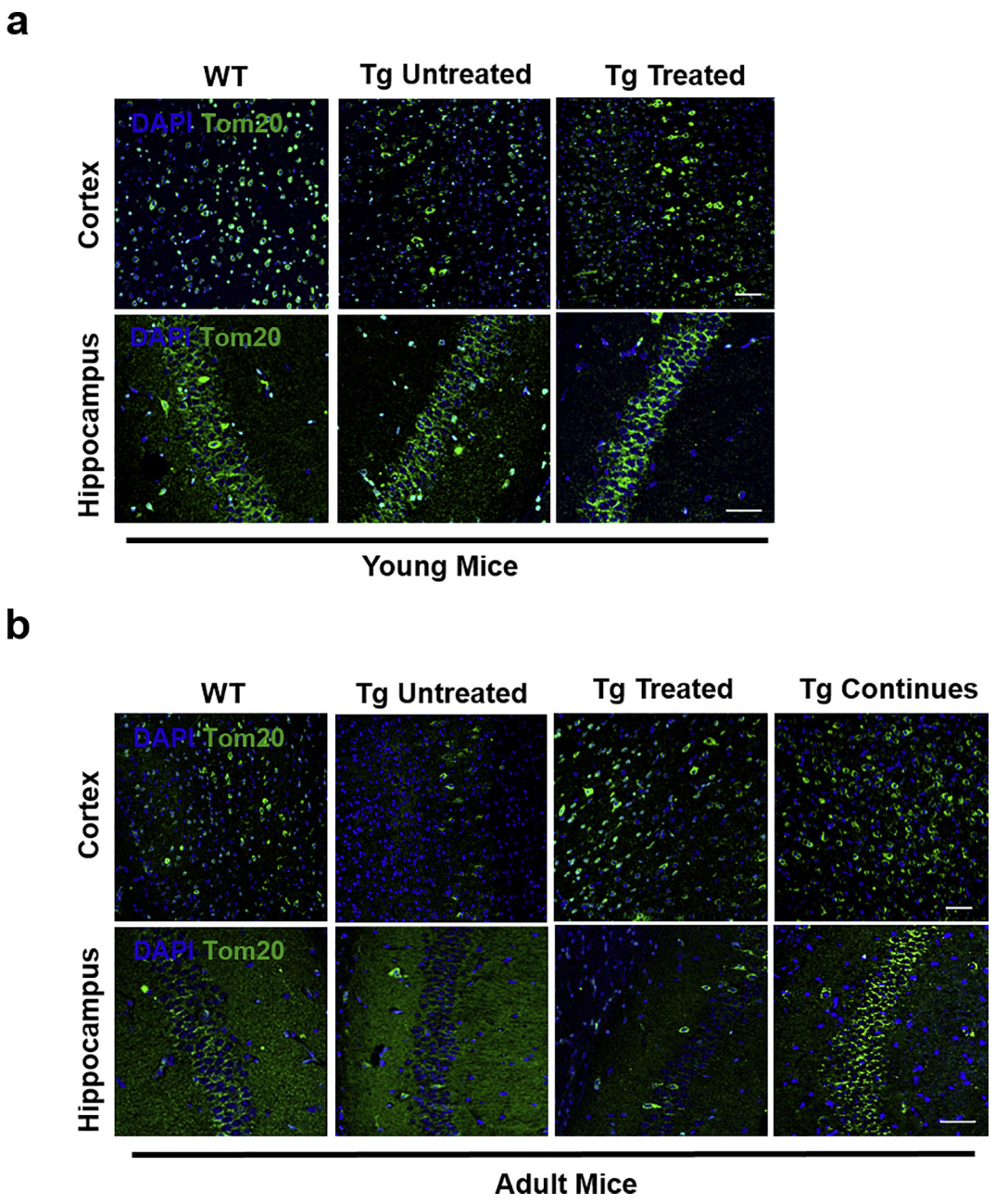

Fig. 2. Reduced levels of TOM20 in older TgMHu2ME199K mice.
Brain sections of wt, untreated TgMHu2ME199K mice as well as Nano-PSO treated TgMHu2ME99K mice were immunostained with an αTom20 antibody (green) and DAPI (blue). (magnification X20, scale bar 100um). (a) young mice (b) adult mice. Pixels of panel b were measured using image pro analyzer 3D software, Media Cybernetics ("Materials and methods" section). The quantification results showed that while for WT sections the percentage of positive area was 3.77 ± 0.11 in cortex and 3.11 ± 1.09 in hippocampus, for the Tg untreated samples, it was 0.3 ± 0.07 in cortex and 0.9 ± 1.23 in hippocampus. Quantification of Nano-PSO Tg treated sections showed 5.38 ± 0.69 in cortex of 2 W treatment and 5.54 ± 0.77 for continues treatment and 1.5 ± 1.11 in hippocampus of 2 W treatment and 3.4 ± 1.29 for continues treatment. (For interpretation of the references to colour in this figure legend, the reader is referred to the web version of this article.)

transcriptional activities of COX subunit genes in neurons (Dhar et al., 2008), and for the expression and activation of NRF2, a transcription factor which controls the expression of a variety of antioxidant and detoxifying enzymes (Ishii et al., 2000; McMahon et al., 2001). Both NRF1 and 2 were also implicated in the expression of the antioxidant response element (ARE)(Biswas and Chan, 2010). Indeed, loss of NRF1 in brain causes age related neurodegeneration (Lee et al., 2011). Interestingly, NRF2 expression is reduced in aging (Zhang et al., 2015), and this may also be true for the activity of NRF1(Mohrin et al., 2015). To learn more about the process of disease initiation vis a vis PrP accumulation in TgMHu2ME199K mice, we correlate the changes in levels of expression (mRNA for NRf1and immunohistochemistry for NRF2) of these transcription factors in wt and TgMHu2ME199K mice to those of disease related PrP accumulation, both by immunohistochemistry (aggregated forms) and by immunoblotting as Protease K (PK) resistant forms.

Fig. 5a shows that very low levels of disease related PrP accumulation can be observed already in newborn TgMHu2ME199K mice brains and subsequently increases so that it is easily detected at both 1.5 and 10.5 months of age. Contrarily, PK resistant PrP forms were detected only several months thereafter (Fig. 5b). This is probably so since the structure of E200K PrP is unstable and thereby prone for

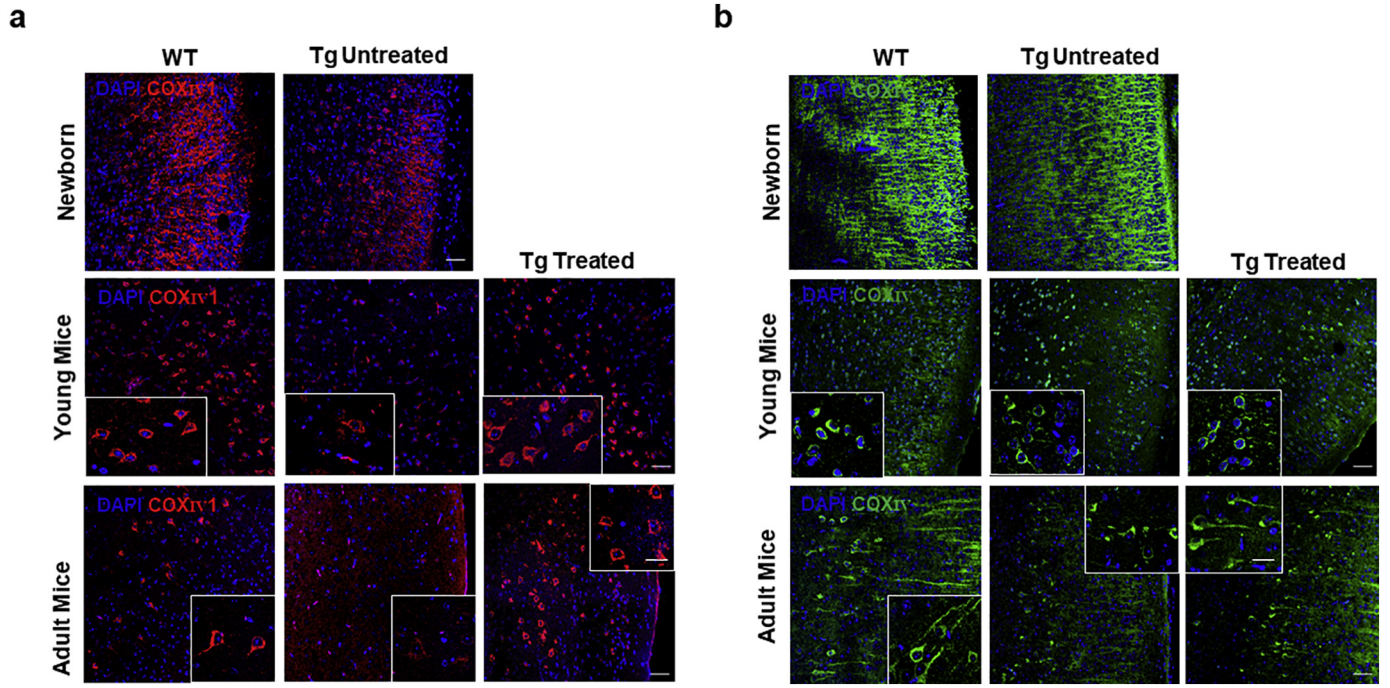

Fig. 3. Reduced COX IV-1 expression in TgMHu2ME199K mice.
Brain slices of newborn, young and adult WT and TgMHu2ME199K, as well as Nano-PSO treated TgMHu2ME199K mice (2 weeks), were immunostained with an α COX IV 1 or α total COX IV antibodies, as described in the methods. The figure shows cortex in all samples. Magnification X20, scale bar 100um; insert in the picture of young and adult mice (magnification X60, scale bar 10um). (a) COX IV1 (red) (b) COX IV (green). In both sections Dapi in blue. Quantification of pixels for COX IV 1 in wt mice were 1.65 ± 0.34 for 1.5 m old and 1.06 ± 0.45 for 9 m old; for tg untreated mice: 0.9 ± 0.13 for 1.5 m old and 0.32 ± 0.09 for 9 m old; for tg treated mice: > 3 for 1.5 m old and 9 m old; Quantification of toal COX IV in wt mice were 1.62 ± 0.41 for 1.5 m old and 1.52 ± 0.56 for 9 m old; for tg untreated mice: 1.67 ± 0.37 for 1.5 m old and 1.37 ± 0.36 for 9 m old; for tg treated mice: 1.4 ± 0.33 for 1.5 m old and 1.63 ± 0.65 for 9 m old; (For interpretation of the references to colour in this figure legend, the reader is referred to the web version of this article.)

aggregation (van der Kamp and Daggett, 2010), but may still require to be oxidized before it converts into a PK resistant form (Canello et al., 2010, 2012; Friedman-Levi et al., 2014; Wang et al., 2016). Both disease related PrP forms (aggregated and PK resistant) increase gradually but then reach a plateau when disease manifestation in TgMHu2ME199K mice is still in its lower scores, regardless of further disease aggravation to a terminal state (Binyamin et al., 2017b; Friedman-Levi et al., 2011). This suggests that early accumulation of aggregated mutant PrP may initiate an oxidative state in the brains of affected mice at very early age.

Concomitantly, Fig. 5c shows that while NRF1 mRNA levels in newborn TgMHu2ME199K mice (12 days), were only marginally reduced when compared to NRF1 levels in wt newborns, young and adult TgMHu2ME199K mice brains presented a significant and similar reduction in NRF1 expression levels. NRF1 levels were not affected by Nano-PSO treatment, suggesting it was not oxidative stress levels in cells, but rather the effect of PrP aggregates on some upstream effector that may result in NRF1 reduced expression (Islam, 2017). These results

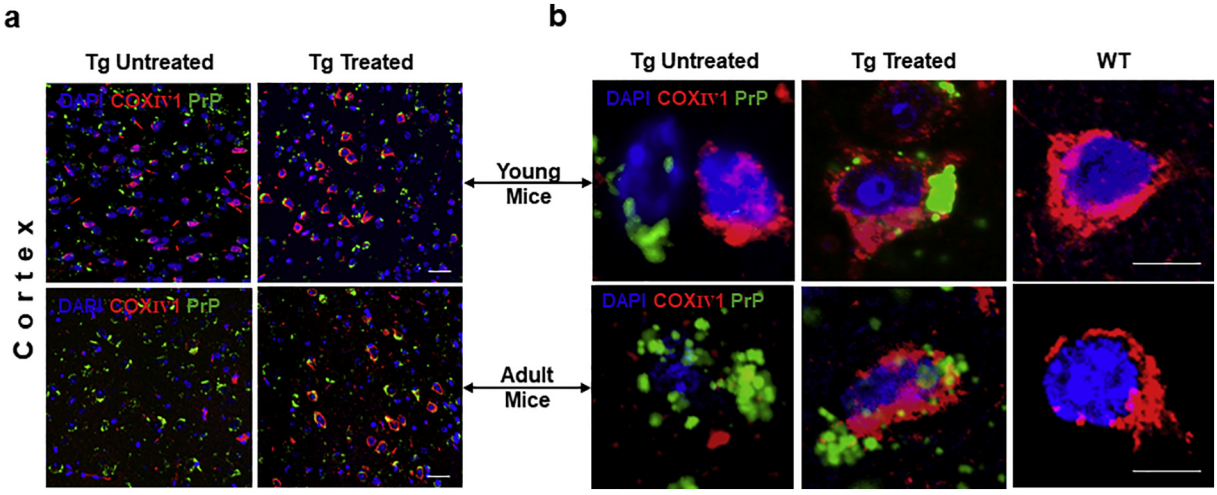

Fig. 4. Nano-PSO administration allows the co-expression of Cox IV1 and disease related PrP.
Brain sections of young and adult Nano-PSO treated and untreated TgMHu2ME199K mice were co-immunostained for COX IV 1(red) and disease related PrP (green). All samples (cortex) were counterstained with DAPI (blue). (a) Magnification x 20 scale bar 50um (b) Also including untreated wt mice sections. Magnification X60, scale bar 10um zoom 3 × 3. (For interpretation of the references to colour in this figure legend, the reader is referred to the web version of this article.)

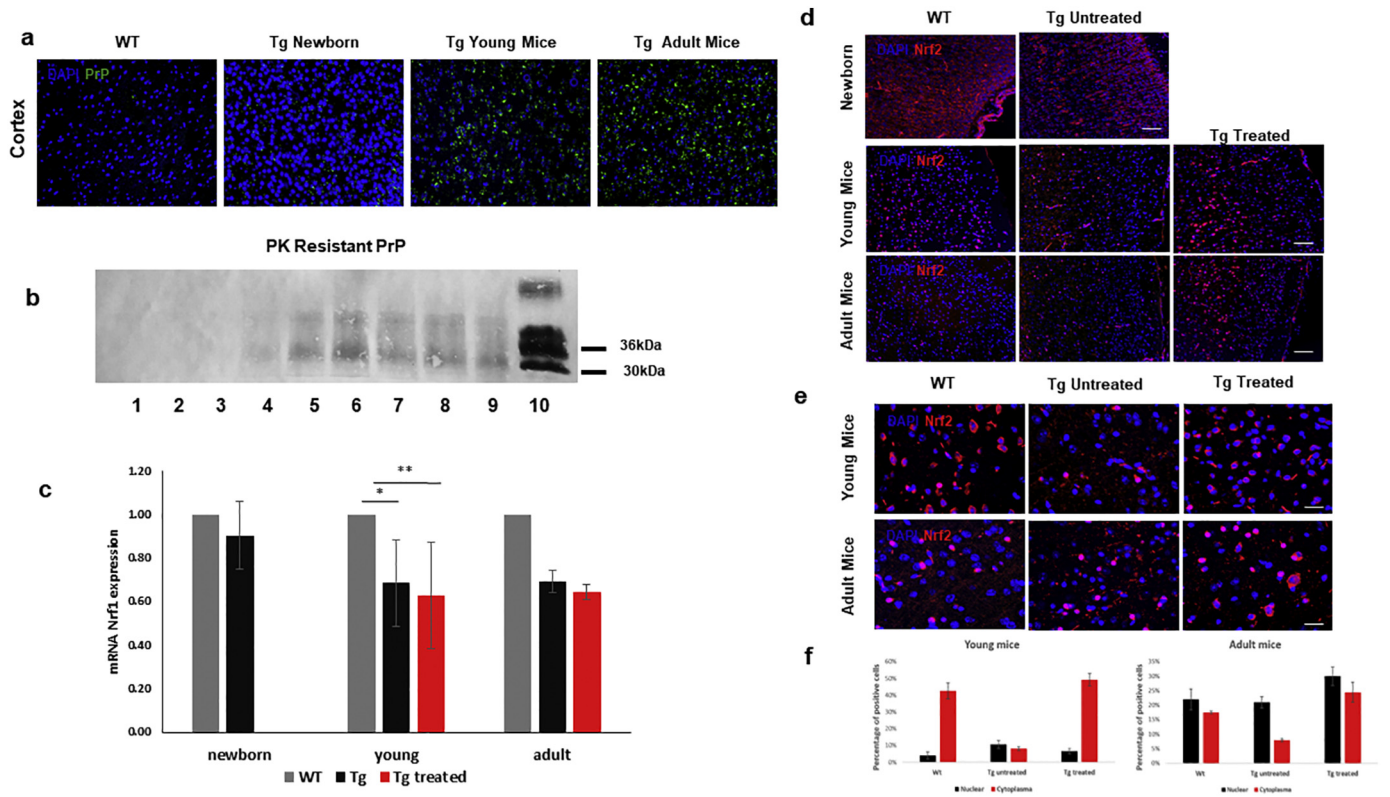

Fig. 5. Accumulation of disease related PrP may induce reduction of NRF1&2 levels.
Brain slices of adult wt, as well as newborn, young and adult TgMHu2ME199K mice were immunostained for disease related PrP (pAb RTC). (magnification x20 scale bar 50um). (b) Brain homogenates from TgMHu2ME199K mice (1: 12d, 2: 1.5 m, 3: 2 m, 4: 4.5 m, 5: 7 m, 6: 9 m, 7: 11 m, 8: 12 m and 9: 14 m), as well as a scrapie infected brain (10) were digested with PK and subsequently immunoblotted with α PrP pAb RTC (c) Real-Time PCR analysis of Nrf1 mRNA expression in brains of newborn, young and adult wt or TgMHu2ME199K mice. Brain RNA samples from TgMHu2ME199K mice were also tested after 2 week treatment with Nano-PSO. Relative expression levels were normalized in reference to UBC. Data are means ± SD (new born $n = 4$/group, WT young $n = 5$, Tg young $n = 6$, Tg young treated $n = 3$, WT adult n = 5, Tg adult n = 4 and Tg adult treated n = 3) $^{*}P < .006$; $^{**}P < .02$. (d) Immunofluorescence detection of Nrf2 (red) in the cortex of newborn, young and adult WT, TgMHu2ME199K and 2 weeks Nano-PSO treated TgMHu2ME199K mice (magnification X20, scale bar 50um) (e) (magnification X40, scale bar 20um) of panel D. (f) Percentage of cells with nuclear and cytoplasmic Nrf2 were counted in the cortex of young and adult mice (n = 4). (For interpretation of the references to colour in this figure legend, the reader is referred to the web version of this article.)

also suggest that the mechanism of Nano-PSO function is mainly to quench ROS chemically, and further signaling may be done by other pathways.

Fig. 5d and e show different magnifications of brain sections from newborn, young and adult wt, as well as treated or untreated TgMHu2ME199K mice immunostained with an αNRF2 antibody. Non activated NRF2 can be observed in cell cytoplasm, while activated NRF2, after its dissociation from Keap 1, can be observed as a strong signal covering the whole nucleus (Esteras et al., 2016). Panel f also shows a quantitative study of both forms of NRF2 performed by counting cells. As shown above for COX-IV1, also NRF2 expression (cytoplasmatic NRF2) was reduced already at 5 day old mice, but more significantly so at 1.5 old months and in adult TgMHu2ME199K mice brains, as compared to both wt and TgMHu2ME199K treated mice. All older mice in these experiments present a large number of activated (nuclear) NRF2 in brains, as previously described (Zhang et al., 2015). This indicates that reduction of ROS levels by Nano-PSO may help activate self-antioxidative Interestingly, it was suggested years ago that PrP binds to NRF2 (Yehiely et al., 1997), but the function of such association was not investigated mechanisms.

3.6. Reduced S20 proteasome levels in adult TgMHu2ME199K brains

While mild oxidative stress is enough to inactivate the 26S proteasome activity, it does not affect the 20S proteasome, which exhibits a high degree a selectivity in degrading oxidized cell proteins (Pickering and Davies, 2012). However, a large body of data indicates that aberrant protein aggregation in neurodegenerative diseases causes inhibition of all proteasome activity (Keller et al., 2000). In prion diseases, it was suggested that a direct contact between PK resistant PrP and the central part of the proteasome, the 20S core particle, results in the inhibition of proteasome activity and subsequent abolishment of mitochondrial turnover and regeneration (Andre and Tabrizi, 2012). Also the reduced expression of Nrf1 and NRF2, as shown above for TgMHu2ME199K mice, may lead to impaired proteasome function (Lee et al., 2011).

To investigate this effect, we examined the expression of the 20S particle in sections from wt, untreated and Nano-PSO treated TgMHu2ME199K mice brains at ages 1.5 and 10.5 months, immunostained with antibodies against the 20S particle and co-stained for COX- IV1 (red) (Fig. 6). We found that in brains from young and asymptomatic TgMHu2ME199K mice, 20S was expressed in cells regardless of reduced COX-IV1 levels. However, the 20S expression was reduced in adult TgMHu2ME199K brains, according with previous findings indicating inhibition of proteasome expression in prion disease (Keller et al., 2000). This figure also shows that reducing ROS levels by Nano-PSO prevents the collapse of the proteasomal system, again explaining the maintained mitochondrial activity (Bragoszewski et al., 2017) and delay in disease progression.

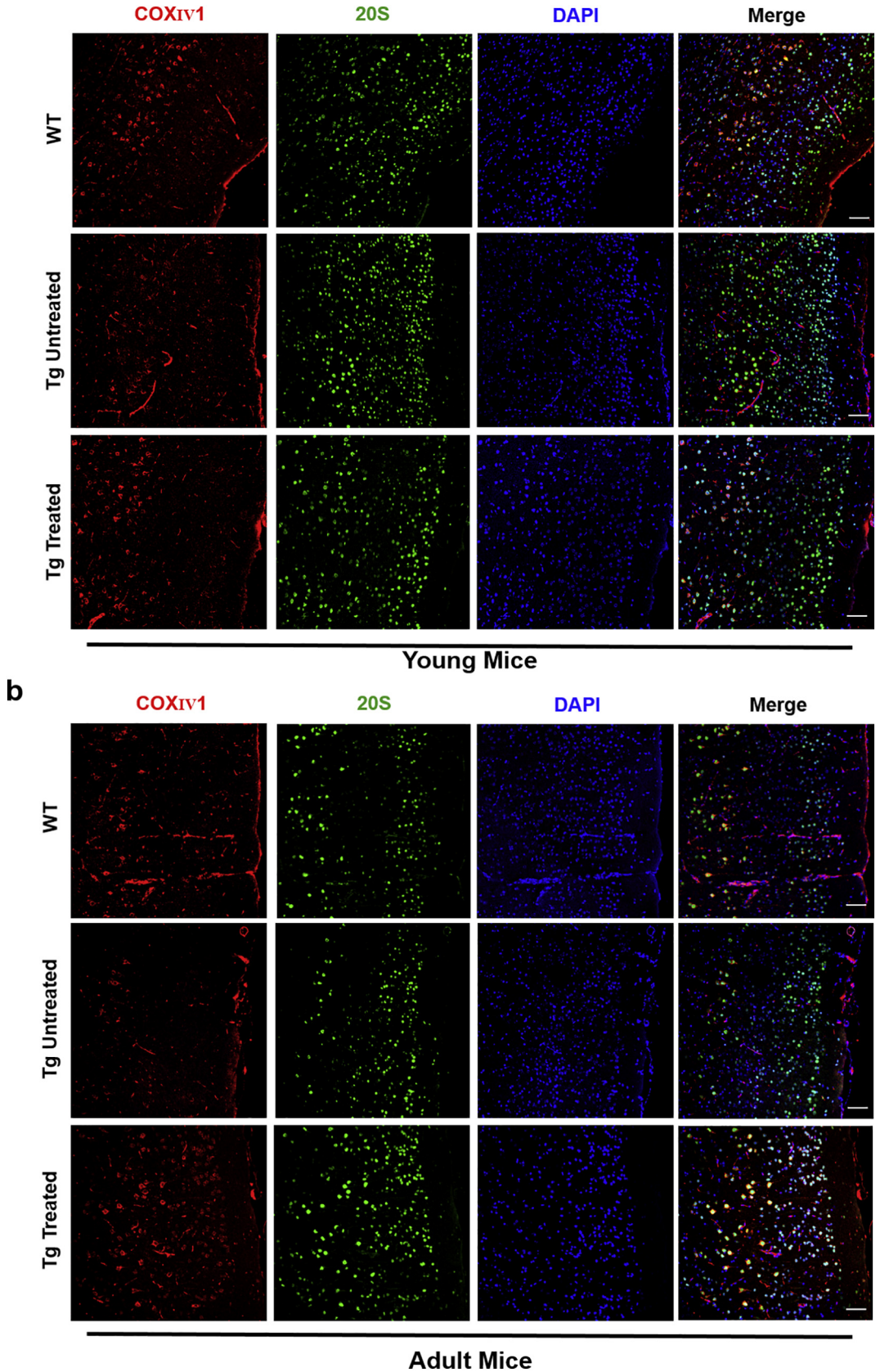

Fig. 6. Reduced S20 proteasome levels in adult TgMHu2ME199K brains.
Brain slices of WT, as well as Nano-PSO treated and untreated TgMHu2ME199K mice, were immunostained for COX IV 1 (red) and the 20S proteasome subunit (green). (magnification X20, scale bar 100um) (a) Cortex of young mice (b) Cortex of adult mice. Quantification of 20S in adult wt was 1.62 ± 0.63; tg untreated 0.62 ± 0.27; tg treated 2.38 ± 0.58. (For interpretation of the references to colour in this figure legend, the reader is referred to the web version of this article.)

4. Discussion

In the genetic forms of neurodegenerative diseases (Kim et al., 2018), dominant germline mutations cause the aberrant folding and accumulation of key disease proteins, resulting in fatal diseases that manifests their first symptoms only decades after birth (Takada et al., 2018). In this project, we set to investigate the biological mechanism underlying late disease onset in subjects at risk, and apply it in the search for treatments that can further postpone the clinical manifestations. Accordingly, we measured the activity and expression of mitochondrial OXPHOS enzymes and oxidation response factors in newborn, asymptomatic and affected TgMHu2ME199K mice (Fainstein et al., 2016; Friedman-Levi et al., 2011), a mouse line mimicking for the E200K PrP mutation linked to CJD in Libyan Jews (Hsiao et al., 1991; Meiner et al., 2012).

We show here that while TgMHu2ME199K mice present the first signs of clinical disease at 5–6 months of age, mitochondrial abnormalities and compensatory mechanisms under oxidative stress, i.e. reduced expression of COX-IV1 and NRF1&2, commenced only days after birth. Reduction of these factors correlated with the initial accumulation of aggregated PrP forms, which start when mice are a few days old, indicating disease related PrP accumulation may induce oxidative stress in cells. It is still to be determined whether mutant PrP may not perform the function of wt PrP. Indeed, while such function is yet to be fully identified, it was suggest to relate to protection from oxidative stress (Bertuchi et al., 2012; Vassallo and Herms, 2003).

The COX IV isoform switch and other unidentified protective mechanisms may preserve the asymptomatic state of the transgenic mice in the presence of increasing levels of disease related PrP accumulation. As explained above, under oxidative stress and degenerative conditions, the CoxIV1 activity is replaced by COX IV-2 (Horvat et al., 2006), resulting in the increase of total COX activity and ATP production. This allows to supply energy to neural cells under pathological conditions (Arnold et al., 1997). However, we hypothesize that further increase in PrP accumulation induces additional oxidative stress to the point of proteasome inhibition, which in turn further inhibits mitochondrial turnover and function. In addition, the reduced expression of both NRF1 and NRF2, factors well known for their role in the transcriptional up-regulation of cytoprotective genes in response to redox stress (Biswas and Chan, 2010), may contribute to the collapse of the protection mechanisms. All these brings the brain cells nearer and nearer to the threshold after which mitochondrial activity is lost and neuronal death commences.

Fig. 7 is a cartoon summarizing the events described above for TgMHu2ME199K mice over time and disease advance. It shows that already in brains of newborn TgMHu2ME199K mice which do not differ in their apparent clinical state from wt mice, there are traces of aggregated PrP as detected by immunohistochemistry, as well as reduced expression of COX IV-1, NRF1 and NRF2. Brains of 1.5 months old TgMHu2ME199K mice present significant accumulation of disease related PrP aggregates, elevated ATP and ROS production as well as activity of OXPHOS enzymes, concomitant with reduced levels of NRF1, NRF2 and COX IV-1 expression, as well as a compensatory mitochondrial response. Even at this time point, there were still no disease signs. These results suggest that in the asymptomatic stages of genetic carriers, the pathological mechanisms of disease may be highly active, as may be the case for the compensatory pathways which may maintain the activity of mitochondria high enough to keep neurons alive. It is only when the levels of disease related PrP are at their maximum that proteasomal function is inhibited and the mitochondrial activity compensation is abolished, resulting in neuronal death and fatal clinical disease.

This putative mechanism suggests several pathways for treatment of genetic prion diseases. First, it implies that treatment should be offered at the asymptomatic stage, while the compensatory mechanisms are still active. After this threshold is passed, it may be difficult to avoid mitochondrial collapse and neuronal death. Moreover, treatments geared to reduce the accumulation of PrP should be given not only very early but need to be extremely efficient, since very low levels of disease related PrP are enough to trigger mitochondrial malfunction, neuronal death and fatal disease. As seen above, low levels of aggregated PrP were enough to induce significant reduction in NRF1, NRF2 and COX IV1 expression. This may be the same for an array of UPR and ARE components that accompanied the asymptomatic stage of prion diseases.

Contrarily, treatments that intend to reduce the levels of ROS in the brain could start at any point, but they may be particularly useful when administration is initiated at the time point in which compensation for mitochondrial activity is about to be lost. As shown here, Nano-PSO, by reducing ROS levels, could restore the expression of COX IV-1 at an early or adult age, even after a short treatment. However, while its clinical effect delaying disease aggravation was the same when treatment started at birth as compared to at 3 months old mice (Binyamin et al., 2017b), treatment during advanced disease may delay advance for a short time but not restore lost neuronal functions (Mizrahi et al., 2014).

This work also contributes an important mechanistic feature of the pathogenesis of prion diseases. It suggest that accumulation of disease related PrP in cells may directly induce oxidative stress, as seen by the fact that the presence of PrP aggregates in cells was incompatible with the expression of COX-IV1. However, co-expression of COX-IV1 and aggregated PrP was possible following Nano-PSO administration, which

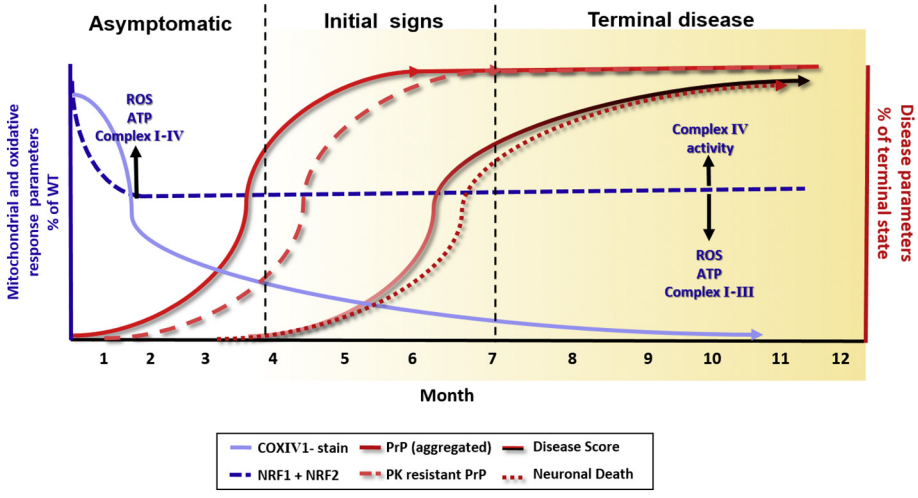

Fig. 7. Mechanism of disease advance in TgMHu2ME199K mice.
This cartoon summarizes the results described in this manuscript. While levels of disease related PrP forms (PK resistant and aggregated) picked at low score of disease, mitochondrial enzymes and oxidation related factors, such as NRf 1 and 2, change their levels of activity of expression very early in the life of the affected mice. Actually, reduction in the levels of COX IV1 and NRF2 initiate concomitant with the appearance of low levels of aggregated PrP.

most probably quenched ROS levels.

5. Conclusions

Our results indicate that while mitochondrial oxidative damage in late onset neurodegenerative conditions, such as genetic CJD, may initiate very early in the life of the mutation carrier, clinical disease appears after such damage can no longer be corrected by oxidative response factors. We also show that brain targeted antioxidants can correct mitochondrial dysfunction and delay onset of the clinical manifestation even in the presence of aberrantly folded PrP.

Funding and acknowledgements

This project was funded by grants from the Agnes Ginges Center for human genetics and from Granalix Biothechnologies. None of these institutions is involves in the planning or the dissemination of the experiments results. We would like to thank Shira Salman Gonen for technical asistance.

References

Andre, R., Tabrizi, S.J., 2012. Misfolded PrP and a novel mechanism of proteasome inhibition. Prion 6, 32–36.
Arnold, S., 2012. Cytochrome c oxidase and its role in neurodegeneration and neuroprotection. Adv. Exp. Med. Biol. 748, 305–339.
Arnold, S., et al., 1997. The subunit structure of cytochrome-c oxidase from tuna heart and liver. Eur. J. Biochem. 248, 99–103.
Ashe, K.H., 2001. Learning and memory in transgenic mice modeling Alzheimer's disease. Learn. Mem. 8, 301–308.
Bertuchi, F.R., et al., 2012. PrPC displays an essential protective role from oxidative stress in an astrocyte cell line derived from PrPC knockout mice. Biochem. Biophys. Res. Commun. 418, 27–32.
Binyamin, O., et al., 2015. Treatment of a multiple sclerosis animal model by a novel nanodrop formulation of a natural antioxidant. Int. J. Nanomed. 10, 7165–7174.
Binyamin, O., et al., 2017a. Continues administration of nano-PSO significantly increased survival of genetic CJD mice. Neurobiol. Dis. 108, 140–147.
Binyamin, O., et al., 2017b. Continues administration of nano-PSO significantly increased survival of genetic CJD mice. Neurobiol. Dis. 108, 140–147.
Biswas, M., Chan, J.Y., 2010. Role of Nrf1 in antioxidant response element-mediated gene expression and beyond. Toxicol. Appl. Pharmacol. 244, 16–20.
Bragoszewski, P., et al., 2017. Control of mitochondrial biogenesis and function by the ubiquitin-proteasome system. Open Biol. 7.
Brown, K., Mastrianni, J.A., 2010. The prion diseases. J. Geriatr. Psychiatry Neurol. 23, 277–298.
Canello, T., et al., 2010. Oxidation of Helix-3 methionines precedes the formation of PK resistant PrP. PLoS Pathog. 6, e1000977.
Canello, T., et al., 2012. Copper is toxic to PrP-ablated mice and exacerbates disease in a mouse model of E200K genetic prion disease. Neurobiol. Dis. 45, 1010–1017.
Cano, M., et al., 2014. Oxidative stress induces mitochondrial dysfunction and a protective unfolded protein response in RPE cells. Free Radic. Biol. Med. 69, 1–14.
Cuervo, A.M., 2008. Autophagy and aging: keeping that old broom working. Trends Genet. 24, 604–612.
Degli Esposti, M., 2002. Measuring mitochondrial reactive oxygen species. Methods 26, 335–340.
van der Kamp, M.W., Daggett, V., 2010. Pathogenic mutations in the hydrophobic core of the human prion protein can promote structural instability and misfolding. J. Mol. Biol. 404, 732–748.
Dhar, S.S., et al., 2008. Nuclear respiratory factor 1 regulates all ten nuclear-encoded subunits of cytochrome c oxidase in neurons. J. Biol. Chem. 283, 3120–3129.
Di Carlo, M., et al., 2012. Are oxidative stress and mitochondrial dysfunction the key players in the neurodegenerative diseases? Free Radic. Res. 46, 1327–1338.
Esteras, N., et al., 2016. Nrf2 activation in the treatment of neurodegenerative diseases: a focus on its role in mitochondrial bioenergetics and function. Biol. Chem. 397, 383–400.
Fainstein, N., et al., 2016. Chronic progressive neurodegeneration in a transgenic mouse model of prion disease. Front. Neurosci. 10, 510.
Faris, R., et al., 2017. Mitochondrial respiration is impaired during late-stage hamster prion infection. J. Virol. 91.
Frid, K., et al., 2018. Autologous neural progenitor cell transplantation into newborn mice modeling for E200K genetic prion disease delays disease progression. Neurobiol. Aging 65, 192–200.
Friedman-Levi, Y., et al., 2011. Fatal prion disease in a mouse model of genetic E200K Creutzfeldt-Jakob disease. PLoS Pathog. 7, e1002350.
Friedman-Levi, Y., et al., 2014. PrP(ST), a soluble, protease resistant and truncated PrP form features in the pathogenesis of a genetic prion disease. PLoS One 8, e69583.
Herbener, G.H., 1976. A morphometric study of age-dependent changes in mitochondrial population of mouse liver and heart. J. Gerontol. 31, 8–12.
Horvat, S., et al., 2006. Effect of hypoxia on the transcription pattern of subunit isoforms and the kinetics of cytochrome c oxidase in cortical astrocytes and cerebellar neurons. J. Neurochem. 99, 937–951.
Hsiao, K., et al., 1991. Mutation of the prion protein in Libyan Jews with Creutzfeldt-Jakob disease. N. Engl. J. Med. 324, 1091–1097.
Ishii, T., et al., 2000. Transcription factor Nrf2 coordinately regulates a group of oxidative stress-inducible genes in macrophages. J. Biol. Chem. 275, 16023–16029.
Islam, M.T., 2017. Oxidative stress and mitochondrial dysfunction-linked neurodegenerative disorders. Neurol. Res. 39, 73–82.
Keller, J.N., et al., 2000. Impaired proteasome function in Alzheimer's disease. J. Neurochem. 75, 436–439.
Kim, M.O., et al., 2018. Genetic PrP prion diseases. Cold Spring Harb. Perspect. Biol. 10.
Kovacs, G.G., Budka, H., 2008. Prion diseases: from protein to cell pathology. Am. J. Pathol. 172, 555–565.
Kovacs, G.G., et al., 2011. Genetic Creutzfeldt-Jakob disease associated with the E200K mutation: characterization of a complex proteinopathy. Acta Neuropathol. 121, 39–57.
Lee, C.S., et al., 2011. Loss of nuclear factor E2-related factor 1 in the brain leads to dysregulation of proteasome gene expression and neurodegeneration. Proc. Natl. Acad. Sci. U. S. A. 108, 8408–8413.
Li, P.A., et al., 2017. Mitochondrial biogenesis in neurodegeneration. J. Neurosci. Res. 95, 2025–2029.
McMahon, M., et al., 2001. The Cap'n'Collar basic leucine zipper transcription factor Nrf2 (NF-E2 p45-related factor 2) controls both constitutive and inducible expression of intestinal detoxification and glutathione biosynthetic enzymes. Cancer Res. 61, 3299–3307.
Meiner, Z., et al., 2012. Tau and 14-3-3 of genetic and sporadic Creutzfeldt-Jakob disease patients in Israel. J. Neurol. 258, 255–262.
Mizrahi, M., et al., 2014. Pomegranate seed oil nanoemulsions for the prevention and treatment of neurodegenerative diseases: the case of genetic CJD. Nanomedicine 10, 1353–1363.
Mohrin, M., et al., 2015. Stem cell aging. A mitochondrial UPR-mediated metabolic checkpoint regulates hematopoietic stem cell aging. Science 347, 1374–1377.
Pickering, A.M., Davies, K.J., 2012. Degradation of damaged proteins: the main function of the 20S proteasome. Prog. Mol. Biol. Transl. Sci. 109, 227–248.
Recasens, A., et al., 2017. In vivo models of alpha-synuclein transmission and propagation. Cell Tissue Res. 373 (1), 183–193.
Redmann, M., et al., 2016. The role of autophagy, mitophagy and lysosomal functions in modulating bioenergetics and survival in the context of redox and proteotoxic damage: implications for neurodegenerative diseases. Aging Dis. 7, 150–162.
Reisch, A.S., Elpeleg, O., 2007. Biochemical assays for mitochondrial activity: assays of TCA cycle enzymes and PDHc. Methods Cell Biol. 80, 199–222.
Rustin, P., et al., 1994. Biochemical and molecular investigations in respiratory chain deficiencies. Clin. Chim. Acta 228, 35–51.
Saada, A., et al., 2003. mtDNA depletion myopathy: elucidation of the tissue specificity in the mitochondrial thymidine kinase (TK2) deficiency. Mol. Genet. Metab. 79, 1–5.
Saada, A., et al., 2004. Evaluation of enzymatic assays and compounds affecting ATP production in mitochondrial respiratory chain complex I deficiency. Anal. Biochem. 335, 66–72.
Scheckel, C., Aguzzi, A., 2018. Prions, prionoids and protein misfolding disorders. Nat. Rev. Genet. 19 (7), 405–418.
Serban, D., et al., 1990. Rapid detection of Creutzfeldt-Jakob disease and scrapie prion proteins. Neurology 40, 110–117.
Shufaro, Y., et al., 2012. Human granulosa luteal cell oxidative phosphorylation function is not affected by age or ovarian response. Fertil. Steril. 98, 166–172.
Takada, L.T., et al., 2018. Prion disease. Handb. Clin. Neurol. 148, 441–464.
Thornton, N., et al., 2010. Two modular forms of the mitochondrial sorting and assembly machinery are involved in biogenesis of alpha-helical outer membrane proteins. J. Mol. Biol. 396, 540–549.
Twig, G., Shirihai, O.S., 2011. The interplay between mitochondrial dynamics and mitophagy. Antioxid. Redox Signal. 14, 1939–1951.
Vassallo, N., Herms, J., 2003. Cellular prion protein function in copper homeostasis and redox signalling at the synapse. J. Neurochem. 86, 538–544.
Walther, D.M., Rapaport, D., 2009. Biogenesis of mitochondrial outer membrane proteins. Biochim. Biophys. Acta 1793, 42–51.
Wang, X., et al., 2014. The effects of NAD+ on apoptotic neuronal death and mitochondrial biogenesis and function after glutamate excitotoxicity. Int. J. Mol. Sci. 15, 20449–20468.
Wang, Z., et al., 2016. Roles of methionine oxidation in E200K prion protein misfolding: Implications for the mechanism of pathogenesis in E200K linked familial Creutzfeldt-Jakob disease. Biochim. Biophys. Acta 1864, 346–358.
Yehiely, F., et al., 1997. Identification of candidate proteins binding to prion protein. Neurobiol. Dis. 3, 339–355.
Zhang, H., et al., 2015. Oxidative stress response and Nrf2 signaling in aging. Free Radic. Biol. Med. 88, 314–336.